JOURNAL OF COMPUTATIONAL PHYSICS 92, 482–507 (1991)

Numerical Modelling of Electromagnetic Casting Processes*

O. BESSON, J. BOURGEOIS, P.-A. CHEVALIER, J. RAPPAZ, AND R. TOUZANI

Département de Mathématiques, Ecole Polytechnique Fédérale, 1015 Lausanne, Switzerland

Received April 4, 1989; revised October 27, 1989

The main goal of this paper is to present a numerical model describing the major physical phenomena involved in electromagnetic casting industrial processes as precisely as possible. Under suitable physical assumptions, we derive the set of equations in the two-dimensional case; we describe in detail the numerical methods used to solve such equations and derive an iterative algorithm. Numerical results describing the case of an aluminium ingot are presented in order to show the efficiency of the method. © 1991 Academic Press, Inc.

1. INTRODUCTION

Electromagnetic casting (EMC) can be schematically described as the making of metal ingots using an industrial set-up where the liquid metal is confined in an electromagnetic field (cf. Fig. 1). This field is induced by an alternating current which flows in the inductor. Solidification is obtained by means of a water jet on the ingot. In most applications, control of the resulting Lorentz forces on the liquid is obtained with a screen. The main advantage of such technology—in contrast with classical casting technologies—is that the faces of the resulting ingot are smoother. A more detailed description of EMC can be found in Refs [1, 2] and the references therein.

The diversity of the physical phenomena observed in EMC make experimental investigations rather heavy and expensive. Therefore, numerical modelling seems to be an efficient alternative to experimentation.

Our purpose, in this paper, is to present a "complete" mathematical model of the two-dimensional problem and to describe the numerical techniques used to solve such equations. Let us point out, furthermore, that even if the model is applied to EMC, the mathematical problem—and the numerical code—handles more general situations, where magnetohydrodynamics (MHD) play a fundamental role. In particular, even though the hydrodynamic contribution in the Ohm law can be

* This research was supported by the Swiss "Commission pour l'Encouragement de la Recherche Scientifique" and the Alusuisse company.

0021-9991/91 $3.00

Copyright © 1991 by Academic Press, Inc.
All rights of reproduction in any form reserved.

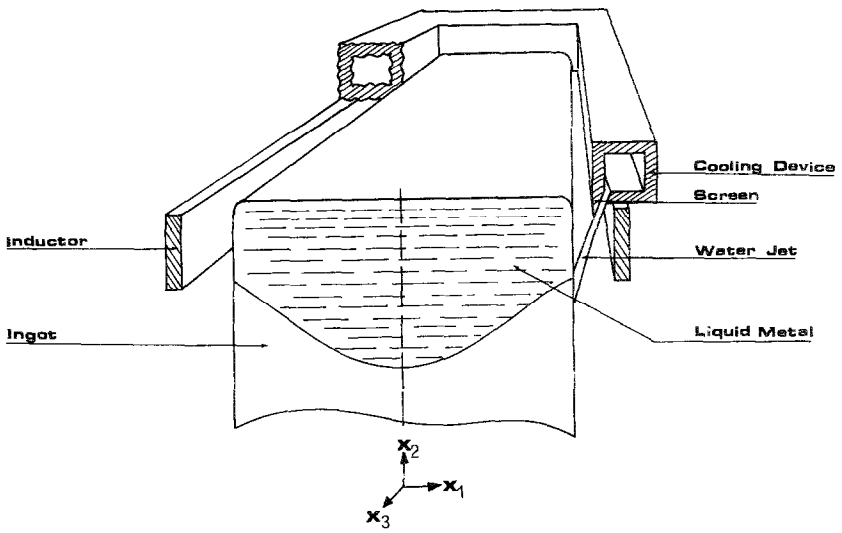

FIG. 1. Schematic representation of the EMC device.

neglected in EMC, the mathematical model and the numerical code take it into account and may therefore be applied to other problems (e.g., electromagnetic stirring).

Numerical modelling of such a problem has already been considered by several authors (cf. [1–4] and the references therein). But, to our knowledge, the new contribution of our work consists in considering the coupling of electromagnetics with hydrodynamics for EMC using boundary integral methods for solving the external electromagnetic problem. Moreover, a common simplification in the literature for this type of models consists in neglecting the surface tension effects in the meniscus. Numerical investigation (cf. Section 6) shows that this effect cannot reasonably be neglected.

The outline of the paper is as follows: In Section 2, we derive the mathematical model using MHD equations and briefly describe an iterative procedure which uncouples the involved problems. In Section 3, the electromagnetic problem is considered. Under some simplifying assumptions, we derive the two-dimensional Helmholtz equation including the convection effect. The approximation of such a problem is performed using a coupled finite element/boundary element method. The hydrodynamic problem is solved in Section 4: the incompressible Navier–Stokes equations are discretized by a classical penalty finite element method. In Section 5, the free boundary problem is investigated and an iteration procedure is set up. Finally, numerical results are given for a cylinder and compared with analytical solutions; the case of electromagnetic casting of aluminium is then simulated.

2. The Mathematical Model

From a physical point of view, EMC involves three main types of phenomena.

(1) An electromagnetic effect created by the inductor. Such a contribution is responsible for the Lorentz force which is assumed to confine the liquid metal. This phenomenon is governed by the Maxwell's equations in the whole space.

(2) Hydrodynamic effects caused by the presence of the Lorentz force. Natural convection resulting from temperature gradient also contributes to the fluid flow. Here, the incompressible Navier–Stokes equations govern the melt flow in the liquid region.

(3) Thermal effects due to the solidification of the liquid metal and to forced convection. The two-phase Stefan equation is usually considered to model these effects; but as we shall see later, these effects are neglected for our purpose.

Further remarks can be made:

(4) Since the meniscus shape (i.e., the interface between the liquid metal and the air) is unknown, a free boundary problem which consists in balancing the involved external forces is therefore to be considered.

(5) Some of the equations considered above are valid only in a subdomain, e.g., the Navier–Stokes equations which are defined in the liquid region.

In order to solve such a coupled problem, some necessary simplifications of the model are introduced. First, since we deal with sufficiently long ingots—in the x_3-direction—we shall adopt a two-dimensional model. More precisely, we assume that all the involved fields are x_3-independent, i.e., translation invariant along the x_3-axis (see Fig. 2 for the example of Aluminium EMC). Furthermore, we shall neglect natural convection effects. Indeed, the present model assumes that the liquidus (i.e., the liquid–solid interface) shape has no effect on the meniscus shape. This assumption has already been made by other authors (cf. [1, 2]). This implies that the heat transfer equation is dropped. More physical assumptions are made on the model and will be introduced when needed.

For such a coupled problem (phenomena (1), (2)), an iterative technique seems to be the natural way to split the problem into "simpler" easy to solve problems. The convergence of the algorithm is checked with respect to the meniscus shape.

In Section 5, we present the flow chart of the iterative procedure in detail; its outline is the following:

1. Give an initial meniscus shape.
2. Solve Maxwell's equations and compute Lorentz forces.
3. Solve Navier–Stokes equations and compute normal tractions on the meniscus.
4. Update the meniscus shape using the Laplace–Young equation.

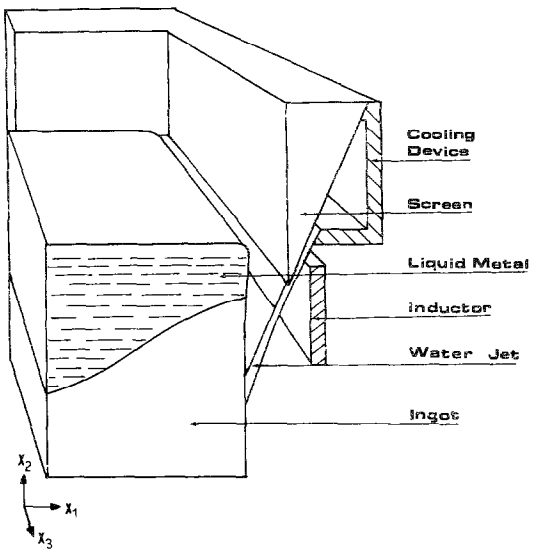

FIG. 2. The "computational" domain.

5. If the meniscus shape is "sufficiently close" to the previous one, then stop; otherwise, go to 2.

In other words, this algorithm consists in uncoupling three types of problems. The next three sections are devoted to the separate investigation of these problems.

3. THE ELECTROMAGNETIC PROBLEM

In this section we are interested in the derivation of the Helmholtz equation which is satisfied by the electromagnetic potential under suitable assumptions. A numerical method to approximate such problem is designed. The method appears as a coupling of finite element and boundary element formulations.

3.1. *Derivation of the Helmholtz Equation*

Consider a set of n infinite cylindrical conductors $A_1, A_2, ..., A_n$ of which the intersections with the plane Ox_1x_2 are denoted by $\Omega_1, \Omega_2, ..., \Omega_n$ and the generating lines are parallel to the x_3-axis. The domains Ω_j, $j = 1, ..., n$ are assumed to be bounded, connected, and disjoined and their boundaries are denoted respectively by $\Gamma_1, \Gamma_2, ..., \Gamma_n$. We set

$$A = \bigcup_{j=1}^{n} A_j, \qquad \Omega = \bigcup_{j=1}^{n} \Omega_j, \qquad \Gamma = \bigcup_{j=1}^{n} \Gamma_j.$$

Let us now assume that these conductors are travelled by an alternating current parallel to the x_3-axis with a moderate frequency f. The system of the n conductors, the permeability of which is supposed to be μ_0, and the vacuum is then governed by the classical Maxwell's equations (cf. [5], for instance) in the whole space $\mathbb{R}^3$:

$$\varepsilon_0 \frac{\partial \mathbf{E}}{\partial t} - \frac{1}{\mu_0} \mathbf{curl}\, \mathbf{B} + \mathbf{J} = 0, \tag{3.1a}$$

$$\frac{\partial \mathbf{B}}{\partial t} + \mathbf{curl}\, \mathbf{E} = 0, \tag{3.1b}$$

$$\varepsilon_0 \operatorname{div} \mathbf{E} = \gamma, \tag{3.1c}$$

$$\operatorname{div} \mathbf{B} = 0. \tag{3.1d}$$

We add the Ohm law to these equations, i.e.,

$$\mathbf{J} = \sigma(\mathbf{E} + \mathbf{u} \times \mathbf{B}) \qquad \text{in } \Lambda, \tag{3.2a}$$

$$\mathbf{J} = 0 \qquad \text{in } \mathbb{R}^3 \setminus \bar{\Lambda}. \tag{3.2b}$$

In the above equations, the time variable is denoted by t, the fields γ, **J**, **B**, **E**, and **u** are defined on $\mathbb{R}^3$ and denote, respectively,

γ, density of charge;

J, electric current;

B, magnetic induction,

E, electric field;

u, velocity of the fluid in the liquid region (by convention, we set $\mathbf{u} = 0$ outside this region).

The physical constants are:

ε_0, dielectric constant of the vacuum;

μ_0, magnetic permeability of the vacuum;

σ, electric conductivity.

We mention at this point that since the electromagnetic problem is uncoupled from the others in the present algorithm, the geometry of the conductors and the velocity **u** of the fluid are assumed to be given data.

The system of Eqs. (3.1)–(3.2) must be understood *in the sense of distributions* over $\mathbb{R}^3$. Let us introduce the following assumptions:

(a) As mentioned already, we are seeking x_3-independent solutions so that Eqs. (3.1)–(3.2) may be considered in $\mathbb{R}^2$ and the involved operators only act on the x_1 and the x_2 variables. We shall denote by $\mathbf{x} = (x_1, x_2)$.

(b) Since we are dealing with alternating currents, we look for periodic electromagnetic fields, i.e., solutions of the form

$$\mathbf{E}(\mathbf{x}, t) = \mathrm{Re}(e^{i\omega t}\mathbf{E}(\mathbf{x})) \qquad \text{in } \Omega, \tag{3.3a}$$

$$\mathbf{B}(\mathbf{x}, t) = \mathrm{Re}(e^{i\omega t}\mathbf{B}(\mathbf{x})) \qquad \text{in } \mathbb{R}^2, \tag{3.3b}$$

where i is the imaginary unit, ω is the angular frequency ($\omega = 2\pi f$) and $\mathrm{Re}(\varphi)$ denotes the real part of a complex-valued function φ. The velocity vector $\mathbf{u}$ is assumed to be stationary.

(c) We assume that the involved fields are of the form

$$\mathbf{B}(\mathbf{x}) = (B_1(\mathbf{x}), B_2(\mathbf{x}), 0) \qquad \text{in } \mathbb{R}^2, \tag{3.4a}$$

$$\mathbf{u}(\mathbf{x}) = (u_1(\mathbf{x}), u_2(\mathbf{x}), 0) \qquad \text{in } \Omega. \tag{3.4b}$$

Note that Eqs. (3.1a), (3.2a), (3.4a), (3.4b) imply

$$\mathbf{E}(\mathbf{x}) = (0, 0, E(\mathbf{x})) \qquad \text{in } \Omega. \tag{3.4c}$$

$$\mathbf{J}(\mathbf{x}) = (0, 0, J(\mathbf{x})) \qquad \text{in } \Omega. \tag{3.4d}$$

(d) We neglect the displacement currents ($\partial\mathbf{E}/\partial t$) in the whole space. This approximation is generally used for moderate frequencies but leads to inaccurate electric field $\mathbf{E}$ in the vacuum.

By virtue of hypotheses (a)–(d), Eqs. (3.1)–(3.2) become

$$-\mathrm{curl}\,\mathbf{B} + \mu_0 J = 0 \qquad \text{in } \mathbb{R}^2, \tag{3.5a}$$

$$i\omega\mathbf{B} + \mathbf{curl}\,E = 0 \qquad \text{in } \Omega, \tag{3.5b}$$

$$\mathrm{div}\,\mathbf{B} = 0 \qquad \text{in } \mathbb{R}^2, \tag{3.5c}$$

$$J = \sigma(E + \mathbf{u} \times \mathbf{B}) \qquad \text{in } \Omega, \tag{3.5d}$$

$$J = 0 \qquad \text{in } \mathbb{R}^2 \setminus \bar{\Omega}, \tag{3.5e}$$

where the symbols "curl" and "**curl**", respectively stand for the scalar curling of a two-dimensional vector field and the two-dimensional vector curling of a scalar field, i.e.,

$$\mathrm{curl}\,\mathbf{B} = \frac{\partial B_2}{\partial x_1} - \frac{\partial B_1}{\partial x_2}, \qquad \mathbf{curl}\,E = \left(\frac{\partial E}{\partial x_2}, -\frac{\partial E}{\partial x_1}\right).$$

Note that Eq. (3.1c) was simply dropped, since its use is to deduce the density of charge γ. Moreover, since $\mathbf{E} = (0, 0, E)$ and $\partial\mathbf{E}/\partial x_3 = 0$, we get from (3.1c) that $\gamma = 0$ in the conductors.

Now from (3.5c) and (3.4a) we deduce the existence of a scalar field $a: \mathbb{R}^2 \to \mathbb{C}$ called *electromagnetic potential*, such that

$$\mathbf{B} = \mathbf{curl}\,a \qquad \text{in } \mathbb{R}^2. \tag{3.6}$$

By (3.5a) and (3.6) we have

$$-\Delta a = \mu_0 J \qquad \text{in } \mathbb{R}^2. \tag{3.7}$$

(i) *In the conductors*, we use the Ohm law (3.5d) and identities (3.6), (3.7) to obtain

$$-\Delta a + \mu_0 \sigma(\mathbf{u} \cdot \nabla a - E) = 0 \tag{3.8}$$

on the one hand. On the other hand, Eqs. (3.5b) and (3.6) give

$$\mathbf{curl}(E + i\omega a) = 0 \qquad \text{in } \Omega,$$

which implies the existence of complex constants C_j such that

$$E + i\omega a = C_j \qquad \text{in } \Omega_j,\ j = 1, 2, ..., n. \tag{3.9}$$

Combining (3.8) and (3.9) yields the equation

$$-\Delta a + \mu_0 \sigma \mathbf{u} \cdot \nabla a + i\omega\mu_0 \sigma a = \mu_0 \sigma C_j \qquad \text{in } \Omega_j,\ j = 1, 2, ..., n. \tag{3.10}$$

(ii) *In the vacuum or air*, Eqs. (3.7) and (3.5e) yield

$$\Delta a = 0 \qquad \text{in } \mathbb{R}^2 \backslash \bar{\Omega}. \tag{3.11}$$

(iii) *On the boundaries of the conductors*, continuity conditions across these boundaries are derived when interpreting Eqs. (3.5) in the sense of distributions and assuming the non-existence of surface currents on the conductors. Namely, from (3.5a) and (3.6) we have

$$\left[\frac{\partial a}{\partial n}\right] = 0 \qquad \text{on } \Gamma, \tag{3.12}$$

where the brackets $[\cdot]$ denote the jump of a function on the curves Γ_j and $\partial/\partial n$ stands for normal derivation. From (3.5c) and (3.6) we deduce that

$$[a] = 0 \qquad \text{on } \Gamma. \tag{3.13}$$

(iv) *At infinity*, the Biot–Savart hypothesis implies that the field $\mathbf{B}$ is an $O(|\mathbf{x}|^{-1})$ when $|\mathbf{x}| \to +\infty$, the real $|\mathbf{x}|$ standing for the euclidean norm of the vector $\mathbf{x}$. This implies that

$$a(\mathbf{x}) = O(\log|\mathbf{x}|) \qquad |\mathbf{x}| \to +\infty.$$

By classical potential theory, the last identity combined with (3.11) implies that

$$a(\mathbf{x}) = d \log|\mathbf{x}| + e + O(|\mathbf{x}|^{-1}), \qquad |\mathbf{x}| \to +\infty, \tag{3.14}$$

where d and e are two complex constants. Without loss of generality, one can choose $e = 0$ since the magnetic induction $\mathbf{B}$ does not depend on e.

Following [6, 7], let us define a new unknown, standing for the normal derivative on Γ, to the problem. Using identities (3.10)–(3.14), the problem consists in finding $a_1 : \Omega \to \mathbb{C}$, $a_2 : \mathbb{R}^2 \backslash \bar{\Omega} \to \mathbb{C}$, $\lambda : \Gamma \to \mathbb{C}$ such that

$$-\Delta a_1 + \alpha \mathbf{u} \cdot \nabla a_1 + i\beta a_1 = \delta \qquad \text{in } \Omega, \tag{3.15a}$$

$$\Delta a_2 = 0 \qquad \text{in } \mathbb{R}^2 \backslash \bar{\Omega} \tag{3.15b}$$

$$a_1 = a_2 \qquad \text{on } \Gamma, \tag{3.15c}$$

$$\frac{\partial a_1}{\partial n} = \frac{\partial a_2}{\partial n} = \lambda \qquad \text{on } \Gamma, \tag{3.15d}$$

$$a_2(\mathbf{x}) = d \log|\mathbf{x}| + O(|\mathbf{x}|^{-1}) \qquad |\mathbf{x}| \to +\infty, \tag{3.15e}$$

where $\alpha = \mu_0 \sigma$, $\beta = \omega \mu_0 \sigma$, and δ is the piecewise constant function which is equal to $\mu_0 \sigma C_j$ on each Ω_j.

In the following, we are concerned with the approximation of problem (3.15).

3.2. *A Variational Formulation*

The main idea consists in representing the potential a_2 (outside Ω) by an integral equation and reformulating problem (3.15) in a bounded domain which can be discretized by a standard Galerkin method.

By the classical potential theory (see Nedelec [8], for instance), Eqs. (3.15b) and (3.15e) yield

$$a_2(\mathbf{x}) = \int_\Gamma \frac{\partial a_2}{\partial n}(\mathbf{y}) G(\mathbf{x}, \mathbf{y})\, ds_y - \int_\Gamma a_2(\mathbf{y})\, G_n(\mathbf{x}, \mathbf{y})\, ds_y, \qquad \mathbf{x} \in \mathbb{R}^2 \backslash \bar{\Omega}, \tag{3.16a}$$

$$\frac{1}{2} a_2(\mathbf{x}) = \int_\Gamma \frac{\partial a_2}{\partial n}(\mathbf{y}) G(\mathbf{x}, \mathbf{y})\, ds_y - \int_\Gamma a_2(\mathbf{y})\, G_n(\mathbf{x}, \mathbf{y})\, ds_y, \qquad \mathbf{x} \in \Gamma, \tag{3.16b}$$

where

$$G(\mathbf{x}, \mathbf{y}) = \frac{1}{2\pi} \log|\mathbf{x} - \mathbf{y}|,$$

$$G_n(\mathbf{x}, \mathbf{y}) = \frac{\partial}{\partial \mathbf{n}_y} G(\mathbf{x}, \mathbf{y}) = -\frac{1}{2\pi} \frac{\mathbf{n}_y \cdot (\mathbf{x} - \mathbf{y})}{|\mathbf{x} - \mathbf{y}|^2}, \qquad \mathbf{y} \in \Gamma,$$

the vector $\mathbf{n}_y$ denoting the outward unit normal to Γ at $\mathbf{y}$. By formally multiplying Eq. (3.16b) by a function μ defined on Γ and integrating over Γ we obtain

$$\int_\Gamma a_2(\mathbf{x}) \mu(\mathbf{x})\, ds_x = 2 \int_\Gamma \int_\Gamma \left(\frac{\partial a_2}{\partial n}(\mathbf{y}) G(\mathbf{x}, \mathbf{y}) - a_2(\mathbf{y})\, G_n(\mathbf{x}, \mathbf{y}) \right) \mu(\mathbf{x})\, ds_y\, ds_x.$$

Let us denote by $H^1(\Omega)$ the usual Sobolev space, $H^{1/2}(\Gamma)$ the space of traces on Γ of functions of $H^1(\Omega)$ and by $H^{-1/2}(\Gamma)$ the dual space of $H^{1/2}(\Gamma)$, all these spaces

being complex-valued. Let us assume $\mathbf{u} \in H^1(\Omega)$. A variational formulation of problem (3.15) consists in seeking $(a, \lambda) \in H^1(\Omega) \times H^{-1/2}(\Gamma)$ such that

$$\mathscr{A}(a, \psi) - \langle \lambda, \psi \rangle = (\delta, \psi) \qquad \forall \psi \in H^1(\Omega), \tag{3.17a}$$

$$\mathscr{B}(\lambda, \mu) + \langle \mu, a \rangle + \langle Ha, \mu \rangle = 0 \qquad \forall \mu \in H^{-1/2}(\Gamma), \tag{3.17b}$$

where

$$\mathscr{A}(a, \psi) = \int_\Omega (\nabla a \cdot \nabla \bar{\psi} + \alpha(\mathbf{u} \cdot \nabla a)\, \bar{\psi} + i\beta a \bar{\psi})\, d\mathbf{x},$$

$(\cdot, \cdot)$, inner product of the space $L^2(\Omega)$,

$\langle \cdot, \cdot \rangle$, duality between $H^{-1/2}(\Gamma)$ and $H^{1/2}(\Gamma)$,

$$\mathscr{B}(\lambda, \mu) = -2 \int_\Gamma \int_\Gamma \lambda(\mathbf{y})\, \bar{\mu}(\mathbf{x}) G(\mathbf{x}, \mathbf{y})\, ds_y\, ds_x,$$

$$Ha = 2 \int_\Gamma a(\mathbf{y})\, G_n(\cdot, y)\, ds_y.$$

Problem (3.17) appears as a *mixed formulation* of the original problem. Existence and uniqueness of a solution of problem (3.17) can be proved by an analogous method to that of [6] provided $\mathbf{u}$ is divergence-free.

Remark. It is clear that if the coefficient β is sufficiently "large"—which is the case for high frequency currents and highly conducting media—then a boundary layer appears. This phenomenon is called in electromagnetic theory *the skin effect.* Its effect on the truncation error, which appears when approximating the problem, can be corrected by refining the mesh near the boundaries. In Ref. [9], asymptotic behaviour of the solution in function of β is derived in the case where $\mathbf{u} = 0$. The results, however, are only valid for conductors with smooth boundaries (i.e., without angles). Another boundary layer appears if the coefficient α is "high." In this case, upwind techniques must be used to avoid oscillations in the numerical solution.

3.3. *Discretization and Matrix Formulation*

Let $\mathscr{T}_h$ be a partitioning of the domain $\bar{\Omega}$ into convex quadrilaterals the diameters of which are not greater than h and let $\mathscr{S}_h$ denote the induced partitioning into segments of the boundary Γ, assumed here to be polygonal for simplicity. We define the finite dimensional spaces,

$$V_h = \{\psi \in C^0(\bar{\Omega}) \mid \psi_{|K} \in Q_1(K)\ \forall k \in \mathscr{T}_h\},$$

$$M_h = \{q \in L^2(\Gamma) \mid q_{|S} = \text{const}\ \forall s \in \mathscr{S}_h\},$$

where $C^0(\bar{\Omega})$ stands for the space of continuous functions over $\bar{\Omega}$ and $Q_1(K)$ is the

space of isoparametrically bi-affine functions on K. After complexification of these spaces, we obtain the obvious inclusions

$$V_h \subset H^1(\Omega), \qquad M_h \subset L^2(\Gamma) \subset H^{-1/2}(\Gamma).$$

The discrete problem consists then in seeking a pair $(a_h, \lambda_h) \in V_h \times M_h$ such that

$$\mathscr{A}(a_h, \psi) - \langle \lambda_h, \psi \rangle = (\delta, \psi) \qquad \forall \psi \in V_h, \tag{3.18a}$$

$$\mathscr{B}(\lambda_h, \mu) + \langle \mu, a_h \rangle + \langle Ha_h, \mu \rangle = 0 \qquad \forall \mu \in M_h. \tag{3.18b}$$

Let us now explicitly define the matrix formulation of problem (3.18). To this end, let N and M denote respectively the number of vertices of the mesh $\mathscr{T}_h$ and the number of element edges lying on the boundary Γ. In addition, let $\{\psi_j\}_{j=1}^N$, $\{\mu_j\}_{j=1}^M$ denote respectively the Lagrange canonical bases of the spaces V_h and M_h. We define the matrices and vectors $[A]$, $[C]$, $[D]$, $[P]$, $\{\delta\}$, $\{a\}$, $\{\lambda\}$ by

$$A_{kl} = \mathscr{A}(\psi_l, \psi_k), \qquad 1 \leqslant k, l \leqslant N,$$

$$C_{kl} = -\int_\Gamma \psi_k \mu_l \, ds, \qquad 1 \leqslant k \leqslant N, \ 1 \leqslant l \leqslant M,$$

$$D_{kl} = \mathscr{B}(\mu_l, \mu_k), \qquad 1 \leqslant k, l \leqslant M,$$

$$P_{kl} = \int_\Gamma H\psi_l \mu_k \, ds, \qquad 1 \leqslant k \leqslant M, \ 1 \leqslant l \leqslant N,$$

$$\delta_k = (\delta, \psi_k), \qquad 1 \leqslant k \leqslant N,$$

$$a_k = a_h(\mathbf{x}_k), \qquad 1 \leqslant k \leqslant N,$$

$$\lambda_k = \lambda_h(\mathbf{s}_k), \qquad 1 \leqslant k \leqslant M,$$

where $\mathbf{x}_k$ is the position of the kth vertex and $\mathbf{s}_k$ stands for an arbitrary point on the kth edge on Γ. Thus, the linear system of equations has the form

$$\begin{pmatrix} [A] & [C] \\ -[C]^{\mathrm{T}} + [P] & [D] \end{pmatrix} \begin{pmatrix} \{a\} \\ \{\lambda\} \end{pmatrix} = \begin{pmatrix} \{\delta\} \\ \{0\} \end{pmatrix},$$

where the $N \times N$-block $[A]$ is a standard *finite element* matrix and has therefore a skyline structure, while the $M \times M$-block $[D]$ is a *boundary element*, hence a dense matrix. The rectangle blocks $[C]$ and $-[C]^{\mathrm{T}} + [P]$ are sparse in the following sense: the entry C_{kl} is zero if the node k does not lie on the boundary Γ. Therefore, it is advantageous to start the numbering of the nodes far from Γ. Hence, we developed a renumbering algorithm which splits the numbering of the internal nodes from boundary nodes (see also [10]). Comparison with traditional finite element renumbering algorithms was favourable to ours.

Let us finally add some remarks on the practical implementation of the method:

(1) The integrals over the elements of $\mathcal{T}_h$ are approximated by means of 2×2-Gauss quadrature.

(2) The boundary integrals are computed *exactly*.

(3) The linear system of equations is stored in a skyline form and solved by the gaussian elimination method.

3.4. *Symmetries of the Solution and Calculation of the Right-Hand Side*

For the particular case of EMC, it is recommended to take into account the symmetry—or the skew symmetry—of the solution with respect to one axis of coordinates. This is simply performed by changing the integral representation of the solution. In Section 6, numerical tests use this method in order to reduce the system dimension.

It is clear that, since the constants C_j in (3.10) are the only data that make it possible to prescribe the injected currents, one shall choose them in such a way that the computed total current density coincides with the prescribed one. We have chosen, therefore, these constants such that:

$$C_j = \begin{cases} 1 & \text{if } \Omega_j \text{ is an inductor,} \\ 0 & \text{otherwise.} \end{cases}$$

We start by calculating the current J_h with the previous constants. The discrete counterparts of Eqs. (3.9), (3.5d), and (3.6) lead to

$$J_h = \sigma(C_j - i\omega a_h - \mathbf{u} \cdot \nabla a_h) \qquad \text{in } \Omega_j.$$

The actual current in the conductors is then replaced by

$$\tilde{J}_h = \frac{\sqrt{2}\, J_0 J_h}{\int_{\text{inductor}} J_h \, d\mathbf{x}},$$

where J_0 is the given *injected* effective current in the inductor. Note that the above *discrete* current is not continuous across the element interfaces.

The above reasoning is not rigorous but is similar to the one used in the three-dimensional case where energetic arguments lead to the same choice (cf. [4]).

4. The Hydrodynamic Problem

We now turn to the fluid flow problem. Let Ω_L denote the liquid region in the domain Ω and assume that Ω_L is connected. The pair $(\mathbf{u}, p)$, where $\mathbf{u}$ and p denote respectively the velocity and the pressure of the fluid, is then a solution to the incompressible stationary Navier–Stokes equations (cf. [5]):

$$-2\,\mathrm{div}\,\mathbf{D}(\mathbf{u}) + \rho\mathbf{u}\cdot\nabla\mathbf{u} + \nabla p = \mathbf{f} + \rho\mathbf{g} \qquad \text{in } \Omega_L, \tag{4.1a}$$

$$\mathrm{div}\,\mathbf{u} = 0 \qquad \text{in } \Omega_L, \tag{4.1b}$$

$$\mathbf{u} = 0 \qquad \text{on } \Gamma_0, \tag{4.1c}$$

$$\mathbf{u}\cdot\mathbf{n} = 0 \qquad \text{on } \Gamma_M, \tag{4.1d}$$

$$\mathbf{s}(\mathbf{u}, p)\cdot\boldsymbol{t} = 0 \qquad \text{on } \Gamma_M. \tag{4.1e}$$

In the above equations, the boundary Γ_L of Ω_L is partitioned into Γ_M and Γ_0, where Γ_M represents the meniscus and Γ_0 is the interface with the solid (cf. Fig. 3), the vector $\mathbf{t}$ denoting the unit tangent vector to Γ_M. The tensor $\mathbf{s}$ is the Cauchy stress tensor

$$\mathbf{s}(\mathbf{u}, p) = 2\mathbf{D}(\mathbf{u})\cdot\mathbf{n} - p\mathbf{n},$$

where $\mathbf{D}$ is the symmetric deformation tensor

$$\mathbf{D}(\mathbf{u}) = \frac{\eta}{2}(\nabla\mathbf{u} + \nabla\mathbf{u}^{\mathrm{T}}).$$

The positive constants η and ρ denote respectively the dynamic viscosity and the density of the fluid. The vectors $\mathbf{f}$ and $\mathbf{g}$ denote respectively the Lorentz and the gravity forces. Condition (4.1d) is a slip boundary condition on the free boundary and condition (4.1e) is a natural Neumann condition.

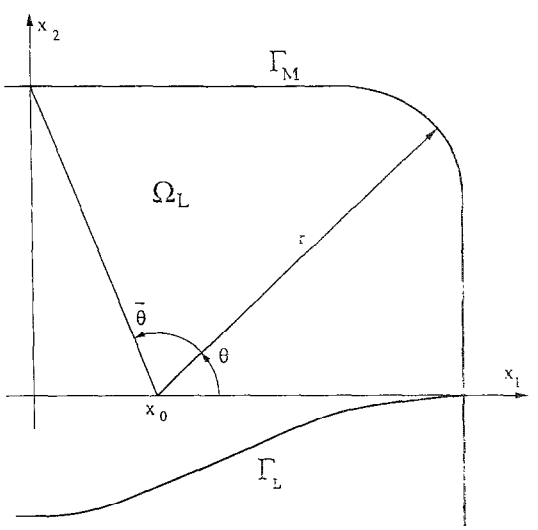

FIG. 3. Curvilinear system of coordinates for the free boundary problem.

4.1. *Calculation of the Body Force*

Again, we assume that the domain Ω and the body force $\mathbf{f}$ are given. Let us express the right-hand side of (4.1a) with respect to the computed electromagnetic potential a.

It is clear that, since we seek steady state flows, the Lorentz body force is to be time-averaged on a period $2\pi/\omega$. Then we have by definition (cf. [5]):

$$\mathbf{f}(\mathbf{x}) = \frac{\omega}{2\pi} \int_0^{2\pi/\omega} \mathrm{Re}(e^{i\omega t}\mathbf{J}(\mathbf{x})) \times \mathrm{Re}(e^{i\omega t}\mathbf{B}(\mathbf{x}))\, dt.$$

Using identities (3.5), (3.6), (3.9), with $C_j = 0$ and the previous definition, we obtain

$$\mathbf{f} = \frac{\sigma\omega}{2}(a_I \nabla a_R - a_R \nabla a_I) - \frac{\sigma}{2}((\mathbf{u}\cdot\nabla a_R)\nabla a_R + (\mathbf{u}\cdot\nabla a_I)\nabla a_I), \tag{4.2}$$

where a_R, a_I denote respectively the real and the imaginary part of the potential a.

Let us notice that even though the force $\mathbf{f}$ involves the velocity vector $\mathbf{u}$, we still assume that this force is known. In view of the iteration process, this means that this force will be evaluated by considering the velocity at the previous iteration. Now, with respect to the numerical approximation of problem (4.1), it is well known that the use of body forces which derive from a potential may induce important numerical errors in classical finite element methods. The cure to the problem

assume that $\mathbf{f} \in (L^2(\Omega_L))^2$. This implies there exist two scalar fields $\varphi, \psi \in H^1(\Omega_L)$ such that

$$\mathbf{f} = \nabla\varphi + \mathbf{curl}\,\psi.$$

The uniqueness of such a decomposition is obtained through the minimization of the L^2-norm of $\mathbf{curl}\,\psi$. One can prove that $\nabla\varphi$ is given by the projection of $\mathbf{f}$ on all the gradients of H^1-functions. Consequently, φ is obtained by solving the boundary value problem: Find $\varphi \in H^1(\Omega_L)/\mathbb{R}$ such that

$$\int_{\Omega_L} \nabla\varphi \cdot \nabla\tilde{\varphi}\, d\mathbf{x} = \int_{\Omega_L} \mathbf{f}\cdot\nabla\tilde{\varphi}\, d\mathbf{x} \qquad \forall\tilde{\varphi} \in H^1(\Omega)/\mathbb{R}. \tag{4.3}$$

The above variational formulation means that, in particular, the solution is known up to an additive constant.

In the sequel, we shall denote by $\mathbf{h}$ the body force field

$$\mathbf{h} = \mathbf{f} - \nabla\varphi,$$

so that Eq. (4.1a) can be written as

$$-2\,\mathrm{div}\,\mathbf{D}(\mathbf{u}) + \rho\mathbf{u}\cdot\nabla\mathbf{u} + \nabla\tilde{p} = \mathbf{h},$$

with

$$\tilde{p} = p - \rho q - \varphi, \qquad \text{where} \quad \mathbf{g} = \nabla q.$$

4.2. *Penalization and Variational Formulation*

In order to take account of the constraint (4.1b), we use a penalty method (cf., e.g., [11]). Moreover, the slip boundary condition is also implemented via a penalty formulation. Numerical experiments show that such a combination of penalty methods works well. More precisely, we formally replace problem (4.1) by

$$-2 \operatorname{div} \mathbf{D}(\mathbf{u}) + \rho \mathbf{u} \cdot \nabla \mathbf{u} - \frac{1}{\varepsilon} \nabla(\operatorname{div} \mathbf{u}) = \mathbf{h} \qquad \text{in } \Omega_L, \tag{4.4a}$$

$$\tilde{p} = -\frac{1}{\varepsilon} \operatorname{div} \mathbf{u} \qquad \text{in } \Omega_L, \tag{4.4b}$$

$$\mathbf{u} = 0 \qquad \text{on } \Gamma_0, \tag{4.4c}$$

$$\mathbf{u} \cdot \mathbf{n} = -\varepsilon \mathbf{s}(\mathbf{u}, \tilde{p}) \cdot \mathbf{n} \qquad \text{on } \Gamma_M, \tag{4.4d}$$

$$\mathbf{s}(\mathbf{u}, \tilde{p}) \cdot \mathbf{t} = 0, \qquad \text{on } \Gamma_M. \tag{4.4e}$$

where $\varepsilon > 0$ is a "small" parameter.

Clearly, the slip boundary condition is implemented as a Robin condition. For more details on such penalty methods, the reader is referred to [12].

Let X be the space of functions of $(H^1(\Omega_L))^2$ which vanish on Γ_0. A variational formulation of problem (4.2) consists in seeking a function $\mathbf{u} \in X$ such that

$$\int_{\Omega_L} \left(2\mathbf{D}(\mathbf{u}) : \mathbf{D}(\mathbf{v}) + (\mathbf{u} \cdot \nabla \mathbf{u}) \cdot \mathbf{v} + \frac{1}{\varepsilon} (\operatorname{div} \mathbf{u})(\operatorname{div} \mathbf{v}) \right) d\mathbf{x}$$

$$+ \frac{1}{\varepsilon} \int_{\Gamma_M} (\mathbf{u} \cdot \mathbf{n})(\mathbf{v} \cdot \mathbf{n}) \, ds = \int_{\Omega_L} \mathbf{h} \cdot \mathbf{v} \, d\mathbf{x} \qquad \forall \mathbf{v} \in X. \tag{4.5}$$

The pressure function is computed from (4.4b) and $p = \tilde{p} + \rho q + \varphi$; it is known up to an additive constant.

4.3. *Discretization*

Using the same mesh $\mathcal{T}_h$ of the domain Ω as in last section, we consider the induced mesh of the domain Ω_L which we denote by $\mathcal{T}_h^L$. Of course, in practice, the "solid" and the "liquid" domains are meshed separately. The space X is then approximated by

$$X_h = \{ \mathbf{v} \in (C^0(\bar{\Omega}_L))^2 \mid \mathbf{v}_{|K} \in (Q_1(K))^2 \ \forall K \in \mathcal{T}_h, \ \mathbf{v} = 0 \text{ on } \Gamma_0 \}.$$

As usual (cf. [11]), the penalty term must be *under-integrated.* We shall not give here the details of the discretized problem since the method is standard.

5. The Free Boundary Problem

5.1. *Generalities*

As in [13, 14], the free boundary is assumed to satisfy the so-called *Laplace–Young* equation which states that the jump of the normal traction on the boundary Γ_M is proportional to the curvature of Γ_M. Namely,

$$\tau\kappa = \sigma_N^2 - \sigma_N^1 \qquad \text{on } \Gamma_M, \tag{5.1}$$

where σ_N^1, σ_N^2 denote the normal tractions on Γ_M calculated on each respective side of Γ_M (liquid and air); the positive constant τ denotes the surface tension of the interface and κ the curvature of the arc Γ_M. Developing the right-hand side of (5.1), we obtain

$$\tau\kappa + \sigma_N + C = 0, \tag{5.2}$$

where σ_N is the normal traction calculated from the Navier–Stokes equations, i.e.,

$$\sigma_N = \mathbf{s}(\mathbf{u}, \tilde{p}) \cdot \mathbf{n} - \varphi - \rho q,$$

in which $\tilde{p}$, φ, and q are determined by choosing a normalization and C is an unknown constant. It now remains to choose an appropriate system of coordinates in order to formulate Eq. (5.2) as an ordinary differential equation. Typically, this depends on the particular problem we are dealing with. In the sequel, we shall choose a system of polar coordinates to localize points of Γ_M, the origin of which is chosen arbitrarily on the x_1-axis. This choice seems to be judicious for the EMC problem (see Fig. 3) and can be furthermore used for other examples. More precisely, for Fig. 3 we have the parametrization of Γ_M:

$$x_1 = x_0 + r(\theta)\cos\theta, \qquad x_2 = r(\theta)\sin\theta, \qquad \theta \in I = [0, \bar{\theta}],$$

where $r(\theta)$ is the unknown function. For this system of coordinates the curvature κ is given by

$$\kappa(r)\colon \theta \in I \mapsto \kappa(r)(\theta) = \frac{r^2(\theta) + 2r'^2(\theta) - r(\theta)\, r''(\theta)}{(r^2(\theta) + r'(\theta)^2)^{3/2}}.$$

If $r = r(\theta)$, $\theta \in I$, is a given function, then its graph gives rise to a meniscus Γ_M and Ω_L is determined. By solving Navier–Stokes equations we obtain a normal traction on Γ_M which is denoted by $\sigma_N(r; \cdot)$; at point θ on Γ_M we shall have the normal traction $\sigma_N(r; \theta)$. With these notations, the equilibrium of Γ_M is given by

$$\tau\kappa(r)(\theta) + \sigma_N(r(\cdot); \theta) + C = 0, \qquad \forall \theta \in I, \tag{5.3}$$

where the constant C and the function $r(\cdot)$ are unknown. Now, since Eq. (5.3) is of the second order, it is clear that boundary conditions must be given for $\theta = 0$

and $\theta = \bar{\theta}$. In addition, the presence of the constant C requires an extra boundary condition. For the present test problem, we choose

$$r'(0) = 0, \qquad r(\bar{\theta}) = \frac{a}{\sin \bar{\theta}}, \qquad r'(\bar{\theta}) = -\frac{a \cos \bar{\theta}}{\sin^2 \bar{\theta}} \quad \text{(see Fig. 3)}, \tag{5.4}$$

where a is a given height of the meniscus. Other kinds of boundary conditions can be supplied for such a problem. In particular, rather than giving the height, one may specify the volume of the liquid region.

5.2. *An Iterative Method for the Resolution of the Free Boundary Problem*

We start by taking a meniscus shape Γ_M^0, the parametrization of which is

$$r = r_0(\theta), \qquad \theta \in I,$$

and we assume that Γ_M^0 is close to the meniscus Γ_M, the parametrization of which is given by

$$r = r_0(\theta) + \xi(\theta), \qquad \theta \in I.$$

Let $C^k(I)$ denote the space of k-times continuously differentiable functions on I. If we define the mapping $F: r \in C^2(I) \mapsto F(r) \in C^0(I)$ by

$$F(r) = \tau \frac{r^2 + 2r'^2 - rr''}{(r^2 + r'^2)^{3/2}},$$

the equilibrium of the meniscus Γ_M is given by (5.3), i.e.,

$$S(\xi) \overset{\text{def}}{=} F(r_0 + \xi) + \sigma_N(r_0 + \xi; \cdot) + C = 0. \tag{5.5}$$

A natural approach would consist in using a Newton method for the resolution of $S(\xi) = 0$. The resulting calculation is however quite complicated because $\sigma_N(r; \cdot)$ is a nonlocal function in r and its derivation with respect to r requires the resolution of an auxiliary boundary value problem. By avoiding the computation of the derivative of σ_N we derive a cheaper iterative scheme for the resolution of (5.5), in the form of the following modified Newton's method:

$$\xi_0 = 0; \tag{5.6a}$$

$$DF(r_0 + \xi_k)(\xi_{k+1} - \xi_k) = -S(\xi_k), \tag{5.6b}$$

$$\xi'_{k+1}(0) = \xi_{k+1}(\bar{\theta}) = \xi'(\bar{\theta}) = 0, \tag{5.6c}$$

with

$$DF(s)\xi = \tau \frac{2s\xi + 4s'\xi' - s''\xi - s\xi''}{(s^2 + s'^2)^3} - 3\tau \frac{(s^2 + 2s'^2 - ss'')(\xi s + \xi' s')}{(s^2 + s'^2)^{5/2}}.$$

In order to improve the convergence of this method, we replace (5.6) by the iterative scheme

$$\xi_0 = 0; \tag{5.7a}$$

$$G(\xi_k)(\xi_{k+1} - \xi_k) = -S(\xi_k), \tag{5.7b}$$

$$\xi'_{k+1}(0) = \xi_{k+1}(\bar{\theta}) = \xi'(\bar{\theta}) = 0, \tag{5.7c}$$

with

$$G(\xi_k) = DF(r_0 + \xi_k) + \mathscr{F}(r_0 + \xi_k),$$

and $\mathscr{F}(r_0 + \xi_k)$ is the radial component of the Lorentz force on the meniscus Γ_M^k described by the function $r_k(\theta) = r_0(\theta) + \xi_k(\theta)$, $\theta \in I$. Let us remark that we obtain $G(\xi_k)$ by the calculation of $S'(\xi_k)$ if we neglect the variation of $\mathbf{s}(\mathbf{u}, \tilde{p}) \cdot \mathbf{n} + \varphi$ with respect to the variation of the curve Γ_M^k.

Let us now recapitulate the iterative procedure for the resolution of the MHD free boundary problem in the following flow chart:

1. Give a domain Ω^0 (and therefore a meniscus shape Γ_M^0);
2. Set $n := 0$;
3. Generate a finite element mesh $\mathscr{T}_h^n$ of the whole domain;
4. Compute the potential a_h^n by (3.18) and the body forces (4.2) in its discrete version;
5. Solve the Poisson equation (Eq. (4.3)) by a Q_1-finite element technique;
6. Solve the Navier–Stokes equations and compute the normal tractions on the meniscus;
7. Update the meniscus shape Γ_M^{n+1} (and therefore Ω^{n+1}) described by (5.7) with a standard finite difference technique;
8. If the meniscus shape is "sufficiently close" to the previous one, then stop;
9. Otherwise, set $n := n + 1$ and go to 3.

Let us notice that:

(1) Step 3 of the algorithm requires no particular computational effort since the remeshing is performed only for the connected component of Ω containing a liquid region. Furthermore, since the meshing algorithm of a domain is based on the subdivision of its boundary, the displacement of this boundary allows an automatic generation of a new mesh.

(2) The solution of the Navier–Stokes equation is performed in the connected component of Ω containing the liquid region. In the solid part of this component we set the velocity to zero, thus saving computer time and memory since boundary conditions are prescribed by removing their corresponding equations from the linear algebraic system.

6. Numerical Results

We present, in this section, two types of runs we have performed with the numerical code. The first, is a simple calculation of an axisymmetric electromagnetic field on a disk. In this case, the analytical solution is known and is used to check the validity of the numerical method. The second test concerns a *schematic* representation of an aluminium electromagnetic caster, the goal being to obtain "realistic" results concerning the validity of the whole model. Let us point out that the real modelization of an EMC device is difficult to obtain because of industrial restriction on such documentation.

6.1. *A Test Problem*

The purpose of this example is to check the electromagnetic field calculation for a case where an analytical solution is known. More precisely, let Ω denote the disk

$$\Omega = \{(x_1, x_2) \in \mathbb{R}^2 \mid (x_1^2 + x_2^2)^{1/2} < R\},$$

and let $\mathbf{u} = 0$ (i.e. static case). Writing Eqs. (3.10) and (3.11) in polar coordinates (r, θ), assuming θ-invariance of the solution and solving the resulting ordinary differential equation, we obtain the solution

$$a_1(r) = BJ_0(\gamma r) - iC/\omega, \qquad a_2(r) = A \log r,$$

where

$$B = \frac{iC}{\omega} \frac{1}{J_0(\gamma R) + \gamma R \log R J_1(\gamma R)}, \qquad A = -B\gamma R J_1(\gamma R),$$

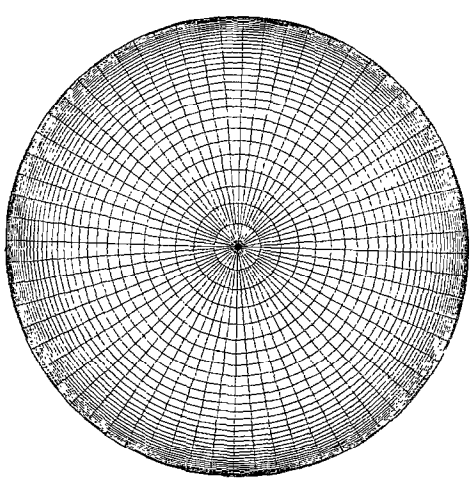

FIG. 4. Finite element mesh of the disk.

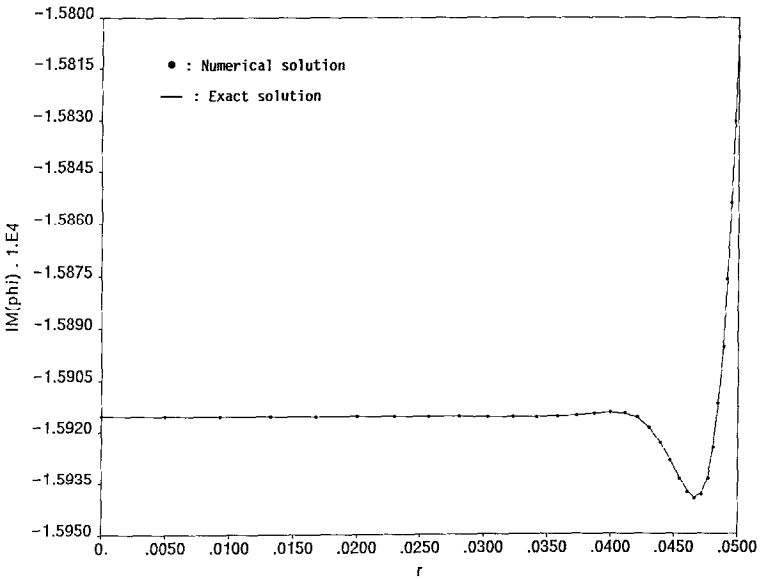

FIG. 5. Potential $\mathrm{Im}(a)$ in function of r for $f = 1000$ Hz.

with the function J_p denoting the pth-order Bessel function and

$$\gamma = (-1 + i)\sqrt{\beta/2}.$$

We tested the electromagnetic part of the code (see Section 3) for

$$\sigma = 0.589 \times 10^8\ \Omega^{-1}\,\mathrm{m}^{-1}, \qquad \mu_0 = 4\pi \times 10^{-7}\ \mathrm{H/m}, \qquad R = 0.05\ \mathrm{m}, \qquad C = 1.$$

Figure 5 shows comparisons between the analytical and the numerical solutions for the frequency $f = 1000$ Hz. A mesh of 1008 elements was generated. Figure 4 shows the mesh used for this test. The density of the mesh near the boundary $r = R$ is required here in order to describe the skin effect precisely.

Figure 6 shows that the rate of convergence for the l_2-norm of the solution vector is two and seems to be optimal.

6.2. *Aluminium EMC*

In this second test, we have designed a rather *schematic* aluminium EMC device. We have sketched on Fig. 7 the various parts of the domain Ω. Namely:

Subdomain	Medium	Conductivity $\sigma[\Omega^{-1}m^{-1}]$
Ω_L	Liquid aluminium	4.083×10^6
Ω_S	Solid aluminium	9.653×10^6
Ω_2	Inductor (copper)	5.89×10^7
Ω_3	Screen (stainless steel)	1.37×10^6
Ω_4	Cooling device (aluminium)	9.653×10^6

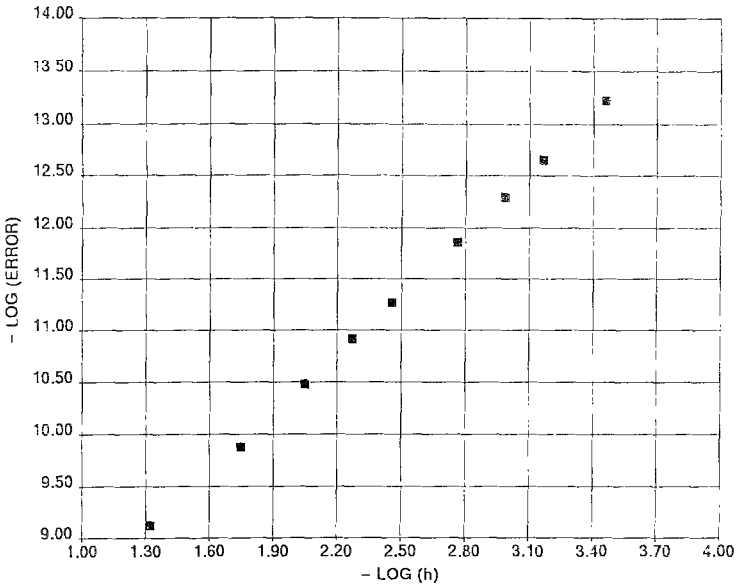

FIG. 6. Rate of convergence of the coupled FEM/BEM on the disk test.

In order to detect hydrodynamical effects, we have run two types of tests with two different frequencies and injected effective currents. Namely,

$$\text{Case I} \qquad J_0 = 6000 \text{ A}, \quad f = 2500 \text{ Hz}.$$

$$\text{Case II} \qquad J_0 = 8000 \text{ A}, \quad f = 50 \text{ Hz}.$$

The other physical data are

$$\mu_0 = 4\pi \times 10^{-7} \text{ H/m}, \qquad \eta = 2.35 \text{ Kg(ms)}^{-1}, \qquad \rho = 2350 \text{ Kg/m}^3, \qquad \tau = 1 \text{ N/m}.$$

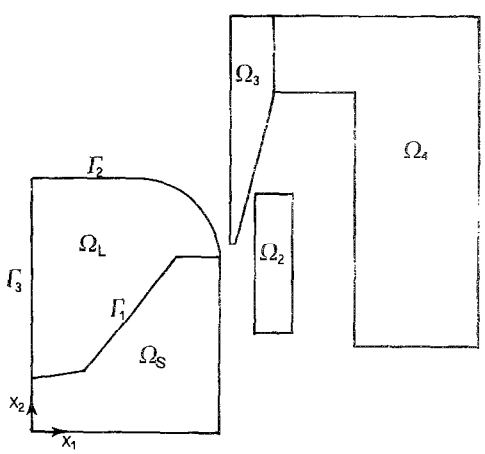

FIG. 7. EMC: detail of the conductors.

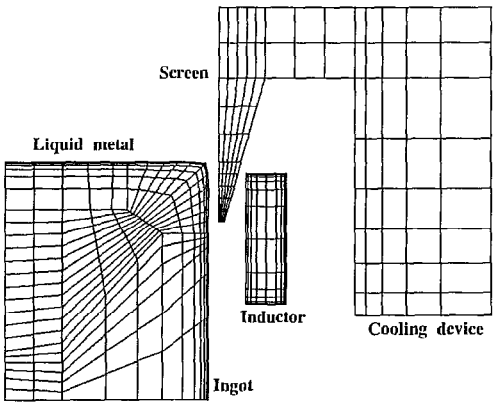

FIG. 8. Initial mesh for the data: $f = 2500$ Hz, $J_0 = 6000$ A (Case I).

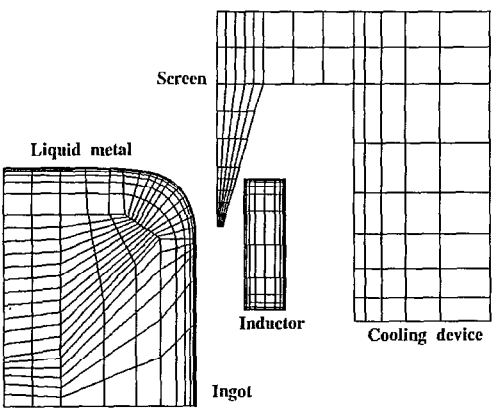

FIG. 9. Final mesh for the data: $f = 2500$ Hz, $J_0 = 6000$ A (Case I).

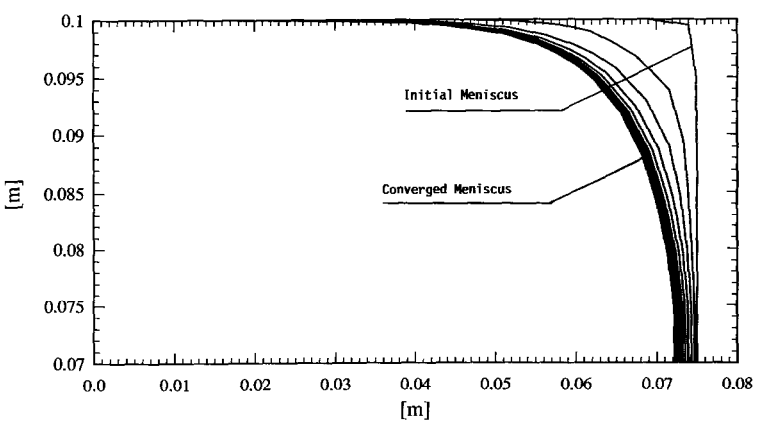

FIG. 10. Iterated meniscus shapes for the data: $f = 2500$ Hz, $J_0 = 6000$ A (Case I).

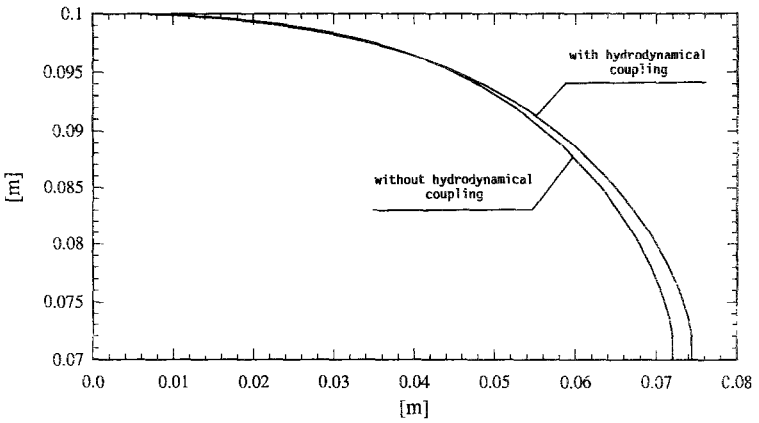

FIG. 11. Meniscus shapes with and without hydrodynamical coupling (Case II).

The boundary conditions for the fluid flow are

$$\mathbf{u} = 0 \qquad \text{on } \Gamma_1,$$

$$\mathbf{u} \cdot \mathbf{n} = 0 \qquad \text{on } \Gamma_2 \cup \Gamma_3,$$

$$\mathbf{s}(\mathbf{u}, p) \cdot \mathbf{t} = 0 \qquad \text{on } \Gamma_2 \cup \Gamma_3.$$

The "initial" and the "final" (after iterations) finite element meshes of the whole domain are represented respectively in Figs. 8 and 9 for Case I. Figure 10 shows the successive meniscus shapes obtained after each iteration for Case I. It turns out that the convergence is reached after 13 iterations, the initial guess being relatively far from the converged solution. In Fig. 11, we have compared the obtained meniscii

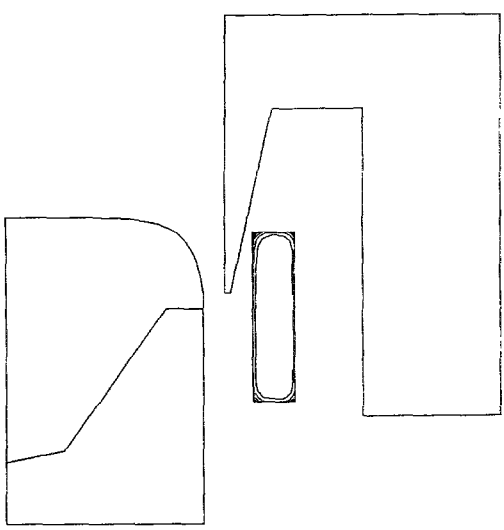

FIG. 12 Contours of modulus of the induced current J_h for Case I.

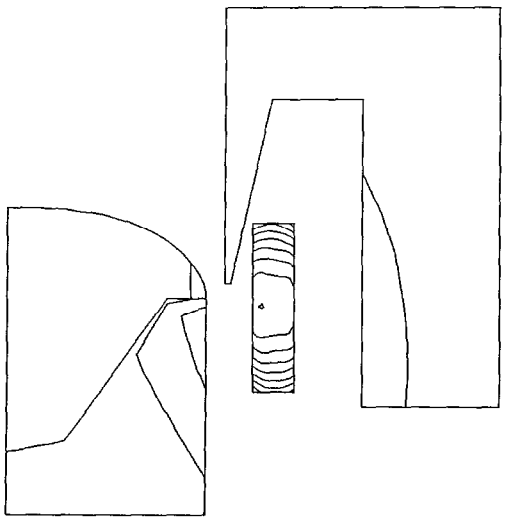

FIG. 13. Contours of modulus of the induced current J_h for Case II.

for Case II with an without taking account of hydrodynamical effects. Clearly, there is a discrepancy of about 3% between the two meniscii.

Moduli of the current field J_h are represented in Figs. 12 and 13 for Cases I and II, respectively. Clearly, the skin effect is well reproduced by numerical simulation.

Figures 14 and 15 show the velocity vectors of the melt flow for both cases, respectively. Here also, as expected, the stirring effect is more visible in the case of low frequency.

The effect of the surface tension of such a meniscus is investigated in Fig. 16 for Case I. It turns out that it is not realistic to neglect such an effect in the equilibrium equation (5.1). Finally, we may notice that:

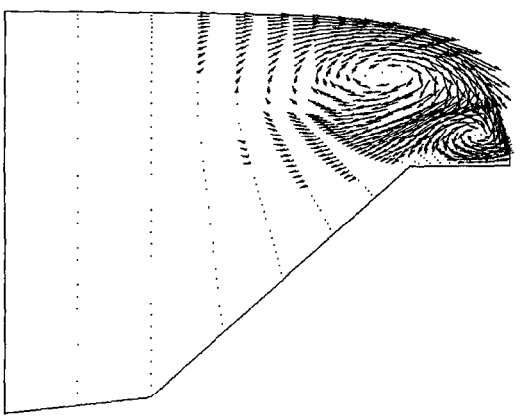

FIG. 14. Velocity of the melt flow for Case I.

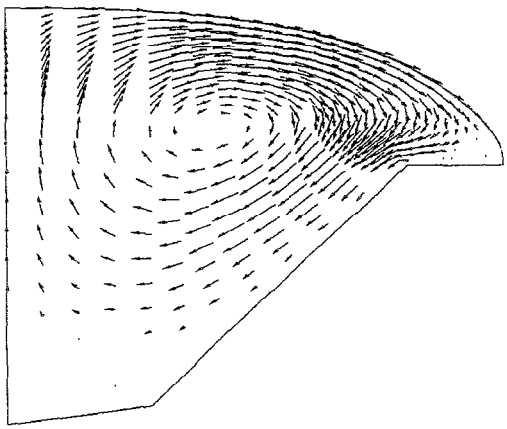

FIG. 15. Velocity of the melt flow for Case II.

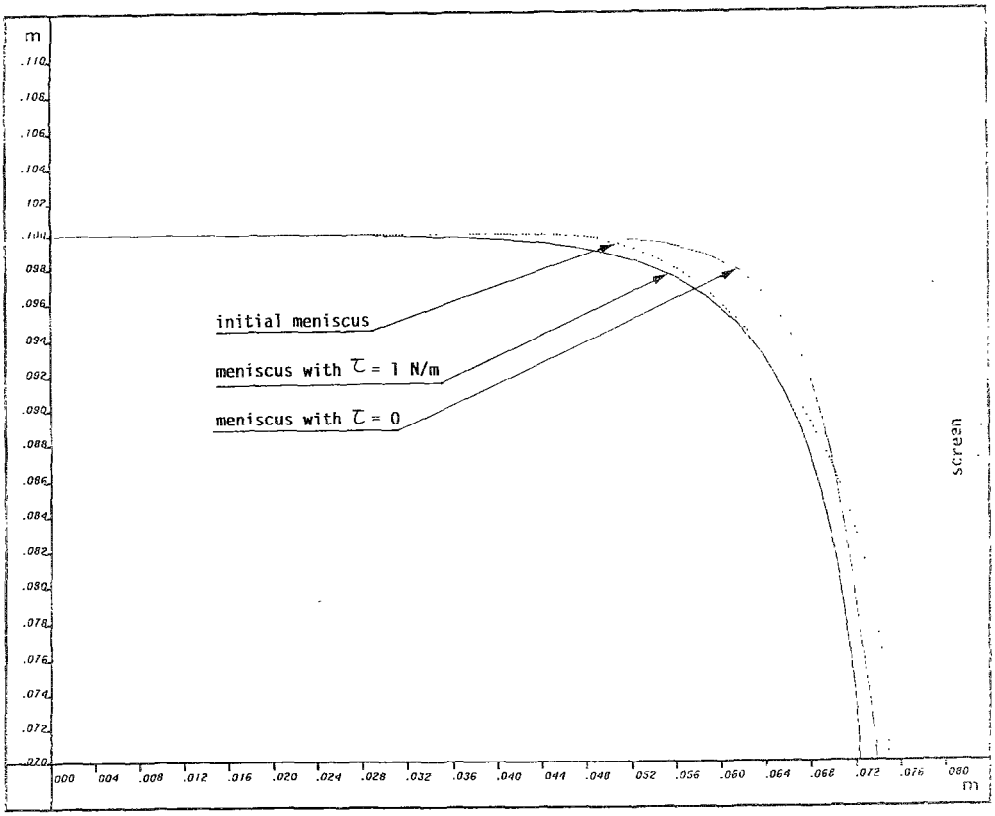

FIG. 16. Meniscus shape in function of the surface tension (Case I).

(1) In the case of high frequency (Case I), the convection effect is really negligible with respect to magnetic and curvature effects. This means that the coupling between the Maxwell and the Navier–Stokes equations is not necessary—at least for the prescribed frequency. This was confirmed by calculation. In fact, the normal tractions are actually negligible—if we remove the hydrostatic part of the pressure. This means that the major part of the Lorentz force derives from a potential which contributes to the stability of the device. This is precisely what one should require for such a technology. The case of low frequencies indicates that when stirring is important (not only in EMC devices), the uncoupling between hydrodynamics and electromagnetics might not always be judicious.

(2) The iteration algorithm of the free boundary problem seems to be quite efficient and cheap.

We conclude by indicating that for this test (as depicted in Fig. 8) each iteration takes about 20 min of CPU time on a Vax 8600 and that convergence is achieved after 10 iterations.

7. Conclusions

The numerical solutions of various systems of partial differential equations arising in two-dimensional MHD problems have been investigated. Numerical methods were derived, which perform well even though they could still be optimized, e.g., by an acceleration of the solvers. The comparisons of the different parts of the code with other methods give satisfactory results.

For the particular case of aluminium EMC, no comparison with experimental data for 2D geometries—in order to test the validity of the model—could be possible since the geometry presented here is only *schematic*.

Acknowledgments

The authors are greatly indebted to Mrs. J. Descloux, P. Maillard (DMA, EPFL), and Mrs. Y. Krähenbühl, R. Von Kaenel, J.-C. Weber (Alusuisse SA) for helpful discussions either on the mathematical formulation or on the physical understanding of the problem.

References

1. J. C. Weber, K. Buxmann, R. Von Kaenel, and M. Plata, *Light Metals*, edited by L. G. Boxall (The Metallurgical Society, Warrendale, PA, 1988), p. 503.
2. J. Sakane, B. Q. Li, and J. W. Evans, *Metall. Trans. B*, **19B**, 397 (1988).
3. A. Glière, P. Massé, and Y. Fautrelle, *IEEE Trans. Magn.* **MAG-24**, 1 (1988).
4. A. Bossavit, *Comput. Methods Appl. Mech. Eng.* **27**, 303 (1981).
5. L. Landau and E. Lifschitz, *Electrodynamics of Continuous Media* (Pergamon, London, 1960).
6. C. Johnson and J.-C. Nedelec, *Math. Comput.* **35**, 1063 (1980).

7. O. ZIENKIEWICZ, D. W. KELLY, AND P. BETTESS, *Int. J. Num. Methods Eng.* **11**, 355 (1977).
8. J.-C. NEDELEC, "Approximation des équations intégrales en mécanique et en physique," internal report, Centre de Mathématiques Appliquées, Ecole Polytechnique, Palaiseau, 1977 (unpublished).
9. M. CROUZEIX AND J. DESCLOUX, *SIAM J. Math. Anal.* **21**, No. 3, 577 (1990).
10. A. BOSSAVIT AND J.-C. VÉRITÉ, *IEEE Trans. Magn.*, **MAG-19**, No. 6, 2465 (1983).
11. T. J. R. HUGHES, W. K. LIU, AND A. BROOKS, *J. Comput. Phys.* **30**, 1 (1979).
12. M. UTKU AND G. F. CAREY, *Comput. Methods Appl. Mech. Eng.* **30**, 103 (1982).
13. C. CUVELIER, "Some Numerical Methods for the Computation of Capillary Free Boundaries Governed by the Navier–Stokes Equations," Technical Report 87-69. TU Delft, 1987 (unpublished).
14. L. LANDAU, AND E. LIFCHITZ, *Fluid Mechanics* (Pergamon, London, 1959).